Contemporary Physics
Vol. 00, No. 00, June 2008, 1–20

RESEARCH ARTICLE

Manifestations of topological effects in graphene

Jiannis K. Pachos[a*]

(*Received 00 Month 200x; final version received 00 Month 200x*)

Graphene is a monoatomic layer of graphite with Carbon atoms arranged in a two dimensional honeycomb lattice configuration. It has been known for more than sixty years that the electronic structure of graphene can be modelled by two-dimensional massless relativistic fermions. This property gives rise to numerous applications, both in applied sciences and in theoretical physics. Electronic circuits made out of graphene could take advantage of its high electron mobility that is witnessed even at room temperature. In the theoretical domain the Dirac-like behavior of graphene can simulate high energy effects, such as the relativistic Klein paradox. Even more surprisingly, topological effects can be encoded in graphene such as the generation of vortices, charge fractionalization and the emergence of anyons. The impact of the topological effects on graphene's electronic properties can be elegantly described by the Atiyah-Singer index theorem. Here we present a pedagogical encounter of this theorem and review its various applications to graphene. A direct consequence of the index theorem is charge fractionalization that is usually known from the fractional quantum Hall effect. The charge fractionalization gives rise to the exciting possibility of realizing graphene based anyons that unlike bosons or fermions exhibit fractional statistics. Besides being of theoretical interest, anyons are a strong candidate for performing error free quantum information processing.

Keywords: Graphene; Topology; Index Theorem; Anyons.

1 Introduction

It is a rare example in science to have theoretical developments and technological applications growing simultaneously at the same rate as with research in graphene [1, 2]. This two dimensional monatomic layer of graphite was theoretically first investigated by Wallace [3]. Experimentally it was successfully isolated at the University of Manchester [4]. Graphene consists of carbon atoms positioned at the vertices of a two dimensional honeycomb lattice. Its electronic properties can be modelled by free electrons that are allowed to tunnel from one site of the honeycomb lattice to a neighboring one. The simple geometrical configuration of the Carbon atoms gives graphene, in the microscopic level, a surprisingly rich collective behavior. The latter is witnessed by quantum effects so resilient that they can influence the behavior of graphene even at room temperature. Due to its unique character graphene can successfully simulate phenomena that are expected to appear in relativistic quantum theories, such as the Klein paradox [5], and it revealed new effects, such is the anomalous quantum Hall effect [6, 7].

The desire to employ graphene for studying topological effects comes from the simplicity with which these effects are encoded in graphene. The Dirac-like description of graphene gives a natural starting point. By varying the geometry of graphene one can create topologically distinct configurations such as a sphere or a torus on which the effective Dirac equation is defined. Moreover, by perturbing the graphene lattice and the tunnelling couplings of the electrons one can give rise to effective gauge and scalar fields. These fields are naturally coupled to the Dirac fermions that model the behavior of graphene. One can encode vortices on the effective scalar field with vorticity determined by the flux of the gauge field going through the vortex, much like

*Corresponding author. Email: j.k.pachos@leeds.ac.uk, URL: quantum.leeds.ac.uk/∼phyjkp [a]*School of Physics & Astronomy, University of Leeds, Leeds LS2 9JT, UK*

ISSN: 0010-7514 print/ISSN 1366-5812 online

DOI: 10.1080/0010751YYxxxxxxxx
http://www.informaworld.com

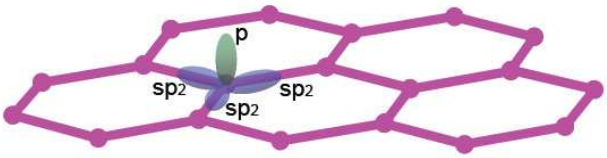

Figure 1. The graphene molecule with a C atom placed at each site of a honeycomb lattice. The electron orbitals of each C atom are depicted. Hybridization provides three equivalent sp_2 orbitals that create the strong σ bonds with the neighboring atoms. This gives rise to the covalent "backbone" of graphene with honeycomb lattice geometry. The remaining $2p_z$ orbital creates a half filled π bond. The latter provides free electrons that tunnel from site to site giving rise to the fascinating electronic properties of graphene.

in superconductors. How the Dirac fermions respond to these topological defects is the central subject of this article.

1.1 *The structure of graphene*

Graphene is a large molecule of carbon atoms, C, that are strongly bound together in a flat configuration. The C atoms are positioned on the sites of a honeycomb lattice, as shown in Fig. 1. Three of the four outer electrons of each carbon atom are employed to strongly bond with its three neighboring atoms via σ bonds. The $2p_z$ orbital of the fourth electron creates a π bond with a neighboring C atoms. The σ bonds provide the covalent "backbone" structure of graphene with honeycomb lattice geometry. Their strength is responsible for the flexibility and robustness of the lattice. The π bonds give rise to graphene's unique electronic structure. Each π bond is half filled allowing the p orbital electrons to tunnel from one atom to the neighboring one. Graphene should be considered as a many body system: several electrons are allowed to tunnel from site to site, while at the same time they satisfy the Pauli exclusion principle. In the following we use this simple model to study the properties of graphene.

1.2 *Topological properties*

Topology is a branch of mathematics that is concerned with the global properties of geometrical objects rather than with their local details. These properties are supposed to be unaffected by continuous deformations of the objects. Restricted in two dimensions we can consider a surface that can be compact, like a sphere or a torus, or it can be open, like a flat sheet or a cylinder. These characteristics are very general and they are invariant even if small geometrical deformations are caused on the surface such as ripples. Compact surfaces can be topologically equivalent to a sphere, or to a torus, if they have a hole, like a ring doughnut. More complicated topologies are possible, too. To distinguish them we assign an integer number called the genus, g, that gives the number of "holes" of each surface. Examples of compact surfaces with genus $g = 0$, $g = 1$ and $g = 2$ are seen in Fig. 2(a), (b) and (c), respectively. It is clear that g is invariant even under deformations of the surface geometry as long as no holes are created or destroyed. In that spirit a cup is topologically equivalent to a ring!

It is a natural question to ask how graphene, a naturally appearing material, can possess such extraordinary properties as the ones related to topology. The main reason is that its chemical bonding is so strong that it induces a stability in the geometrical properties of the underlined lattice. Indeed, several stable geometric variants of graphene appear in nature. In all of them each carbon atom has precisely three neighbors. The lattice of these molecules mainly consists of hexagons with a number of additional pentagons or heptagons that induce curvature. For example, one can encounter cylinders (Fig. 2(d)), so called nanotubes, produced from a folded graphene sheet, with the number of open faces, N, being equal to two. Spherical configurations are also possible (Fig. 2(a)) the so called fullerenes with $N = 0$. The same geometry is also met in the football, where twelve pentagons are present in between the hexagonal plaquettes so that a spherical configuration can be created. It is also possible to have crossing nanotubes

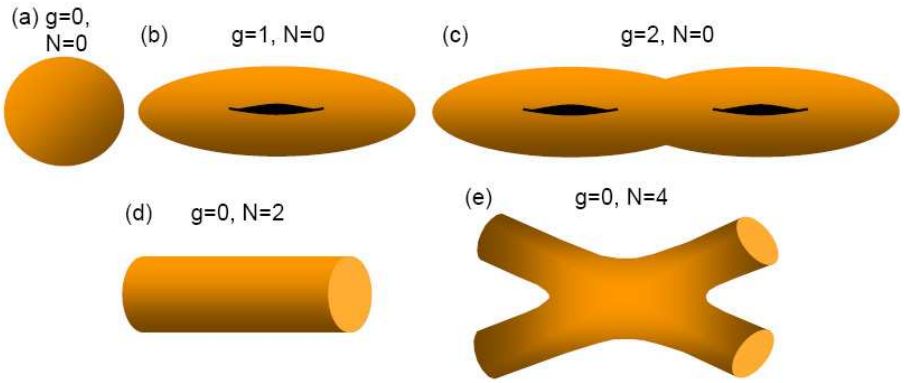

Figure 2. Two dimensional surfaces with different topologies characterized by the genus, g, or the number of open faces, N. The surfaces (a), (b) and (c) are compact with $N = 0$ and $g = 0$, 1 and 2, respectively. The surfaces (e) and (d) are open with $g = 0$ and $N = 2$ and 4, respectively.

corresponding to a surface with four open faces, as seen in Fig. 2(e). Apart from the robust geometrical structure of the underlined lattice, the presence of long range quantum coherences are also responsible for the emergence of the topological character in graphene. Indeed, at low enough temperatures one can assume that graphene's electrons can travel coherently through the whole molecule, thus detecting its geometry or topology. This makes graphene the natural laboratory to study the interplay between topology and quantum physics.

1.3 *The index theorem*

Classical as they may be, topological configurations can have a dramatic effect on the quantum behavior of a system. In particular, they determine the possible quantum states a system can have. This striking connection is demonstrated by the index theorem, initially introduced by Atiyah and Singer in the sixties [8]. The index theorem provides a direct way to determine certain properties of the spectrum of general Hamiltonians. Its application is rather straightforward providing a good alternative to the direct diagonalization of the Hamiltonian. This can be a tantalizing task for large systems. It is, therefore, not hard to imagine that the index theorem can have a dramatic impact on theoretical and applied sciences [9, 10].

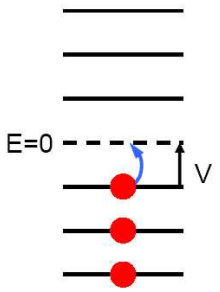

Figure 3. The energy levels of a fermionic system are considered here to be symmetric around $E = 0$. For half filling systems there are half as many fermions as there are possible states. The lowest energy is obtained by occupying the negative energy states with a single fermion due to the Pauli exclusion principle. The application of a properly tuned potential difference, V, can cause the system to change its state, if there are zero modes to be occupied. This will give rise to an electric current. In the absence of zero modes no change will be observed and the system will appear as an insulator.

In particular, the index theorem provides information about the number of zero energy states that are present in systems such as graphene and its geometric variants [11, 12]. They are important for determining conductivity properties. To understand why let us look closer at the nature of these molecules. It is common that the employed Hamiltonians have symmetric spectra around zero energy, called the particle-hole symmetry. The negative part of the spectra

is called valence band and the positive part conducting band. As mentioned above, graphene has approximately half as many free electrons as the positions they can occupy. Due to the Pauli exclusion principle these electrons fill up the valence band states one by one until the zero energy point. This point corresponds to half of the possible occupation positions. When adding a small potential difference one can witness conducting or insulating behavior depending on the presence of zero modes. If there are zero modes then they can be occupied in response to the electric field. This change in the electronic states appears macroscopically as a current. If there are no zero modes the small shift in the energy will cause no change in the behavior of the system, thus appearing as an insulator.

Apart from the conducting properties, the presence of zero modes can give rise to exotic characteristics. It can be shown by general arguments that vortices encoded on graphene can cause the fractionalization of charge. This collective behavior is known from the fractional quantum Hall effect. Drawing the analogy further, the vortices in graphene could actually be possessing fractional anyonic statistics, which is neither similar to bosons nor fermions [13]. It is an exciting possibility to have a physical system that needs mainly isolation from the environment to reveal such fascinating properties. Experiments that reveal such aspects of topological behavior are usually hard to perform due to the complexity needed for topological properties to arise. Graphene, however, could achieve this with minimal requirements.

2 Elementary properties of graphene

As we have seen, graphene is a molecule consisting of C atoms arranged on a two dimensional honeycomb lattice. The elementary plaquette of the lattice is a hexagon and the atoms are placed on the sites of the lattice. Graphene's electronic properties can efficiently be described by the tight binding model, where spinless electrons tunnel from site to site along the links of the lattice without interacting with each other. This simple model provides a surprisingly accurate description of graphene and gives rise to a wealth of phenomena. The tight binding Hamiltonian is given by

$$H = -J \sum_{\langle \mathbf{i},\mathbf{j} \rangle} (a^\dagger_{\mathbf{i}} a_{\mathbf{j}} + a^\dagger_{\mathbf{j}} a_{\mathbf{i}}), \tag{1}$$

where the operator $a^\dagger_{\mathbf{i}}$ creates an electron at site $\mathbf{i}$, $a_{\mathbf{j}}$ annihilates it at $\mathbf{j}$ and the coupling J gives the strength of the tunnelling transition. To determine the spectrum of Hamiltonian (1) we take advantage of its periodicity. For that we notice that the system repeats itself with respect to a unit cell that comprises of two neighboring sites, e.g. along the $\mathbf{v}_3$ vector, as seen in Fig. 4. This periodic structure allows us to perform a Fourier transformation that reduces the energy

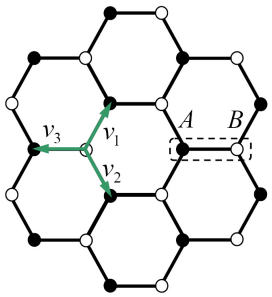

Figure 4. Graphene can be modelled by a honeycomb lattice, where electrons are tunnelling from site to site. This lattice has hexagons as the elementary plaquettes. It can be split into two triangular sublattices, indicated by black and white circles and denoted here by A and B, respectively. The doted rectangular denotes the unit cell of the lattice.

eigenvalue problem to the diagonalization of the Hamiltonian in a single unit cell. Indeed, for

$a(\mathbf{k}) = \sum_{\mathbf{i}} e^{i\mathbf{k}\cdot\mathbf{i}} a_{\mathbf{i}}$ we obtain

$$H = -J \iint d^2k \left(a_A^\dagger(\mathbf{k}), a_B^\dagger(\mathbf{k})\right) \begin{pmatrix} 0 & \sum_{i=1}^3 e^{i\mathbf{k}\cdot\mathbf{v}_i} \\ \sum_{i=1}^3 e^{-i\mathbf{k}\cdot\mathbf{v}_i} & 0 \end{pmatrix} \begin{pmatrix} a_A(\mathbf{k}) \\ a_B(\mathbf{k}) \end{pmatrix}, \tag{2}$$

where $a_A(\mathbf{k})$ and $a_B(\mathbf{k})$ correspond to the Fourier transformed operators that are positioned on the left and on the right of the unit cell, respectively. Now, it is straightforward to find the eigenvalue of the energy for electrons with certain momentum. This only requires diagonalizing the two by two matrix inside the integral and yields

$$E(\mathbf{k}) = \pm J \sqrt{1 + 4\cos^2 \frac{\sqrt{3}k_y}{2} + 4\cos\frac{3k_x}{2}\cos\frac{\sqrt{3}k_y}{2}}. \tag{3}$$

Common as they might look, these energy eigenvalues possess a unique property. They become zero for isolated points of momentum. These are called Fermi points and are positioned at $\mathbf{K}_\pm = 2\pi/3(1, 1/\sqrt{3})$. The presence of Fermi points makes the low energy behavior of graphene so special. At half fermionic filling and at zero external potential graphene is at zero energy in the sense that the valence band is completely filled. In this case the behavior of graphene is dominated by the behavior of the Hamiltonian (2) near the Fermi points. To determine this

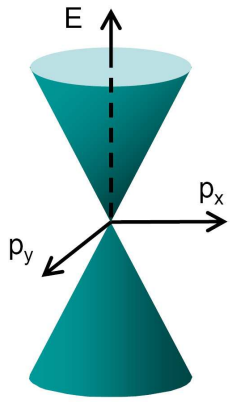

Figure 5. The spectrum, E, of graphene near a single Fermi point as a function of the small momenta, p_x and p_y. The conical shape corresponds to a linear relation between the energy and the momentum that characterizes the Dirac equation. The positive spectrum corresponds to the conducting band and the negative to the valence band.

behavior we substitute $\mathbf{k} = \mathbf{K}_\pm + \mathbf{p}$, expand the Hamiltonian in powers of $|\mathbf{p}|$ and take into account only the first order terms by assuming that $|\mathbf{p}|$ is small. This gives the equation

$$\begin{pmatrix} H_+ & 0 \\ 0 & H_- \end{pmatrix} \Psi(\mathbf{r}) = \begin{pmatrix} \boldsymbol{\sigma}\cdot\mathbf{p} & 0 \\ 0 & (\boldsymbol{\sigma}\cdot\mathbf{p})^* \end{pmatrix} \Psi(\mathbf{r}) = \boldsymbol{\gamma}\cdot\mathbf{p}\Psi(\mathbf{r}) = E\Psi(\mathbf{r}), \tag{4}$$

where $\mathbf{p} = -i\hbar\boldsymbol{\nabla}$, $\boldsymbol{\sigma} = (\sigma^x, \sigma^y, \sigma^z)$ are the Pauli matrices and $H_\pm$ is the Hamiltonian kernel that corresponds to each Fermi point $\mathbf{K}_\pm$. Moreover, $\boldsymbol{\gamma}$ are the Dirac matrices given by

$$\boldsymbol{\gamma} = \begin{pmatrix} \boldsymbol{\sigma} & 0 \\ 0 & -\boldsymbol{\sigma}^* \end{pmatrix} \tag{5}$$

and for simplicity we have set $3J/2 = 1$. Eqn. (4) shows that, due to the presence of isolated Fermi points, the low energy behavior of graphene can be described by a relativistic Dirac operator, $\not{D} = \boldsymbol{\gamma}\cdot\mathbf{p}$, with energy dispersion relations given in Fig. 5. The corresponding eigenvectors are

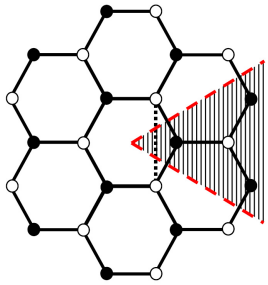

Figure 6. The introduction of curvature on a flat sheet of graphene by cutting a $\pi/3$ sector centered at the middle of a hexagon and gluing the opposite ends. This, finally, creates a cone that has positive curvature. The resulting lattice has a single pentagon at the apex of the cone, while the rest of the plaquettes remain hexagonal.

four dimensional spinors, $(|\,\mathbf{K}_+A\rangle\,,|\,\mathbf{K}_+B\rangle\,,|\,\mathbf{K}_-A\rangle\,,|\,\mathbf{K}_-B\rangle)^T$, where the components are the wave functions of the unit cell elements A and B for each of the Fermi points $\mathbf{K}_\pm$.

It is surprising that these effective Dirac fermions do not have any mass term. This fact is responsible for the high mobility properties of graphene. The presence of the Fermi points is responsible for the semi-metallic behavior of graphene. That is, it behaves as metal due to the vanishing gap between the valence and conducting bands, as seen in Fig. 5, but with charge carriers in small numbers due to the vanishing density of states at the Fermi level. Finally, there are emerging pseudo-spin degrees of freedom, where the Pauli matrices are acting, as we initially started with spinless electrons.

Of course, we have not discovered a fundamental relativistic field. We have only shown that the collective behavior of graphene electrons can be described by the Dirac equation. Indeed, the obtained effective velocity of the electrons is three hundred times smaller than the speed of light, c. The relativistic description of graphene's electrons gives rise to numerous new phenomena that can be tested in the laboratory, like the Klein paradox [5], the anomalous integer quantum Hall effect [7] and so on.

2.1 *Curvature effect*

The next theoretical surprise is related to the way curved graphene is described. As may be naturally expected the low energy description of a curved graphene surface is given by a Dirac equation that is defined on the corresponding curved surface. But this is not the full story. The curvature induces an effective gauge field that needs to be introduced in the Dirac equation. The latter is equivalent to an actual gauge field with magnetic field flux going through the molecule surface. This is a remarkably simple way to couple gauge fields to Dirac fermions.

To understand the mechanism that gives rise to the gauge fields let us examine how one can insert curvature to graphene. The simplest way is by cutting a $\pi/3$ sector from a graphene sheet and then gluing the opposite ends of the lattice, as seen in Fig. 6. This process adds a single pentagon at the apex of the created cone. All the other plaquettes remain hexagonal. This minimal geometrical distortion of the honeycomb lattice adds positive curvature. The curvature can be measured by circulating a tangential vector, $\mathbf{T}$, around the apex, i.e.

$$\oint \mathbf{T}\cdot d\mathbf{r} = \frac{\pi}{3}. \tag{6}$$

But this is not yet the end of the story! The insertion of a single pentagon forces us to connect two sites that are of the same type, e.g. B for the case in Fig. 6. This is different compared to the flat graphene, where every site A has only B neighbors or via versa. This discontinuity has a dramatic effect on the corresponding spinor that describes the deformed lattice. Indeed, when the spinor, Ψ, is transported around the apex by an angle 2π it is forced at some point to jump from a site B to a site B instead of a site A. This reminds us of the effect that a magnetic

field has on the wave function of an electron moving on a closed path. A full circulation gives a phase factor to the electron wave function that is proportional to the enclosed magnetic flux. This effect is known as the Aharonov-Bohm effect [14]. Quantum mechanically, the magnetic field introduces a discontinuity: the wave function of the electron should simultaneously describe the processes of the electron remaining static or spanning a closed trajectory. This is rectified by introducing a vector potential term in the Hamiltonian that makes the theory consistent. Following similar steps one needs to add a non-Abelian vector potential term, $\mathbf{A}$, in the effective Hamiltonian description of the curved graphene that compensates the jump in the components of the spinor, Ψ. The circulation of $\mathbf{A}$ along a loop, C, around the apex is given by

$$\oint_C \mathbf{A} \cdot d\mathbf{r} = \frac{\pi}{2}\tau^y, \tag{7}$$

where τ^y is the second Pauli matrix that mixes the $\mathbf{K}_+$ and $\mathbf{K}_-$ components of the spinor. This fascinating emergence of the effective gauge field is simply caused by the geometric distortion of the graphene lattice. The manifestation of the gauge potential is witnessed by the properties of geometric variants of graphene, such as the spherical fullerenes, and it is in the core of the topological effects described here.

The resulting Hamiltonian includes the curvature effect and a non-Abelian gauge field that couples the Fermi points, $\mathbf{K}_+$ and $\mathbf{K}_-$. It is possible to rotate this Hamiltonian so that the gauge field reduces to two Abelian fields that act independently on each Fermi point. In this rotated frame the effective Hamiltonian is given by

$$H = \begin{pmatrix} -ie_k^\mu \sigma^k (\nabla_\mu - ieA_\mu) & 0 \\ 0 & ie_k^\mu \sigma^k (\nabla_\mu + ieA_\mu) \end{pmatrix}. \tag{8}$$

The covariant derivative is given by $\boldsymbol{\nabla} = \boldsymbol{\partial} - i\boldsymbol{\Omega}$, where $\boldsymbol{\Omega}$ is the spin connection that describes the effect of curvature on the vector character of the spinors. It has circulation

$$\oint_C \boldsymbol{\Omega} \cdot d\mathbf{r} = -\frac{\pi}{6}\sigma^z, \tag{9}$$

where σ^z acts on the A and B components of the spinor and C is a loop around the apex of a cone. The Abelian gauge potential satisfies

$$\oint_C \mathbf{A} \cdot d\mathbf{r} = \frac{\pi}{2}, \tag{10}$$

with the corresponding magnetic field given by $\mathbf{B} = \boldsymbol{\nabla} \times \mathbf{A}$. The zweibeins, e_k^μ, are introduced to make the Hamiltonian covariant in the induced curved space. If the curved space, with metric $g^{\mu\nu}$, has coordinates x^μ and the local flat space, with metric η^{kl}, has coordinates ξ^k then the zweibeins are defined by $e_k^\mu = \partial x^\mu / \partial \xi^k$ and they satisfy $g^{\mu\nu} = e_k^\mu e_l^\nu \eta^{kl}$. Practically, the zweibeins transform the Pauli matrices from the flat to the curved space in order to be contracted with the corresponding covariant derivative. From the metric $g_{\mu\nu}$ one can define the corresponding Christoffel symbols, $\Gamma^\sigma_{\mu\nu} = \frac{1}{2} g^{\sigma\rho}(\partial_\mu g_{\nu\rho} + \partial_\nu g_{\mu\rho} - \partial_\rho g_{\mu\nu})$, while the scalar curvature is given by

$$R = g^{\mu\nu} R^\rho{}_{\mu\nu\rho}, \text{ where } R^\mu{}_{\nu\rho\sigma} = \partial_\sigma \Gamma^\mu_{\nu\rho} - \partial_\rho \Gamma^\mu_{\nu\sigma} + \Gamma^\lambda_{\nu\rho}\Gamma^\mu_{\lambda\sigma} - \Gamma^\lambda_{\nu\sigma}\Gamma^\mu_{\lambda\rho}. \tag{11}$$

The final Dirac equation, $H\Psi = E\Psi$, where H is given in (8), describes the behavior of a Dirac spinor, Ψ, coupled to a gauge field, $\mathbf{A}$, on a surface with curvature R. This model approximates well the low energy behavior of the carbon molecules [15, 16, 17, 18, 19], which corresponds to states with large wavelength. The lattice spacing appears to be small for these states and the continuous limit can be safely taken. To be precise, the continuous limit corresponds to the limit

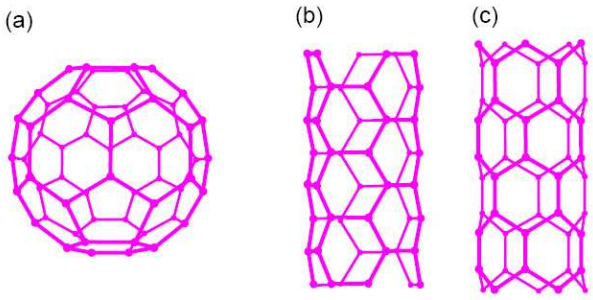

Figure 7. (a) The C60 fullerene molecule, where there are 12 pentagons necessary to produce the spherical configuration. Nanotube of armchair type (b) and of zigzag type (c). It is not necessary to introduce pentagons for producing nanotubes as they have zero curvature.

of infinitely large molecules, where states with arbitrarily large wavelength can be supported. Nevertheless, we will see that the continuous approximation describes graphene molecules well even for relatively small lattices. Hamiltonian (8) has all the necessary ingredients that are responsible for the topological character of graphene molecules. It is now of interest to see what specific form the Dirac equation takes for the various geometric deformations of graphene.

3 Geometric variants of graphene

Among the most common geometrical variants of graphene are the fullerene [20] and the nanotubes [21]. Fullerenes, also known as buckyballs, are compact molecules with zero genus. As a representative, the C60 has sixty carbon atoms positioned in a spherical configuration, as seen in Fig. 7(a). In order to create the curvature of the sphere one has to introduce twelve pentagons on an initially flat sheet of hexagons. This is the case for all buckyballs of arbitrary size as we shall explicitly see in the next section. On the contrary nanotubes are just folded graphene sheets in a cylindrical configuration. Nanotubes have zero two dimensional curvature so there is no need for the presence of any pentagons. Due to their lattice structure there are many distinct ways in which a nanotube can be folded. Each one is characterized by different boundary conditions. Examples are the armchair (Fig. 7(b)) and the zigzag configuration (Fig. 7(c)).

Of course, one can imagine more complex molecules with positive as well as negative curvature. Negative curvature is present, for example, at saddle points and can be introduced by heptagons. The latter introduce an effective magnetic field flux that is exactly opposite to the one corresponding to pentagons. By employing pentagons and heptagons, one can generate any desirable graphene surface. These include compact surfaces of arbitrary genus as well as open ones. In the following we consider only open surfaces that can be produced by a normal section of compact ones. An example is the nanotube that is produced from a torus by cutting it along its smallest circle.

The Hamiltonian that describes the low energy spectrum of each of these molecules is given by a Dirac equation similar to the one in (8). Now the metric, $g_{\mu\nu}$, describes the curvature of the surface of each molecule. The gauge field, $\mathbf{A}$, is responsible for the local magnetic flux through every polygonal deformation. Thus, by keeping track of the geometry of the surface of the molecule as well as its polygonal deformations one is able to construct the corresponding Dirac operator that describes its low energy limit. Tedious as it may seem there is a simple way to determine the total flux going through the molecule from its general topological characteristics. This is achieved with the aid of the Euler theorem, which is presented in the following section.

4 Euler theorem

As we have seen, to establish the low energy description of graphene molecules we need to determine the total number of plaquette deformations. If we know the total number of pentagons and heptagons present in a molecule of certain genus, then we can determine the total flux that goes through the molecule. There is a simple way to relate the number of these deformations to the topology of the corresponding molecule. Indeed, the Euler theorem [22] gives a relation between the structural details of a polyhedral lattice and its total topological properties. There are numerous proofs of this theorem, the most pedagogical ones are based on a reduction of the polyhedral lattice to simpler ones without changing its topological properties.

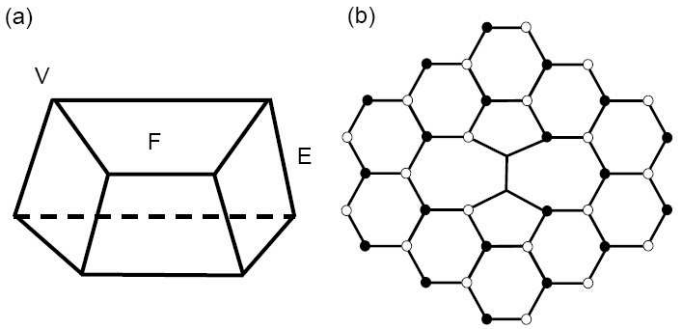

Figure 8. (a) A simple lattice corresponding to genus zero surface, where the vertices, V, edges, E, and faces, F, are depicted. (b) Two pentagonal and two heptagonal deformation can be introduced on graphene lattice without changing its flat geometry.

Consider a lattice that lies on a surface that we initially take to be compact of a certain genus, g. An example of such a lattice with genus $g = 0$ is seen in Fig. 8(a). Let V, E and F be the number of vertices, edges and faces of the lattice, respectively. The Euler characteristic, χ, is given by

$$\chi = V - E + F = 2(1 - g), \tag{12}$$

where the second equation consists the Euler theorem. We now apply this theorem to the case of graphene molecules. Each graphene vertex has exactly three links. Let us assume that only pentagonal or heptagonal deformations are present. Denote by n_5, n_6 and n_7 the total number of pentagons, hexagons and heptagons in the molecule. Then the total number of faces is given by the sum of the different polygons, $F = n_5 + n_6 + n_7$. The total number of vertices is given by $V = (5n_5 + 6n_6 + 7n_7)/3$ as each k-gon has k vertices and each vertex is shared by three polygons. Similarly, the total number of edges is given by $E = (5n_5 + 6n_6 + 7n_7)/2$ as each edge is shared by two polygons. Substituting this into Eqn. (12) we obtain

$$n_5 - n_7 = 12(1 - g). \tag{13}$$

There are many characteristics that spring out from this result. If equal numbers of pentagons and heptagons are inserted then they do not change the topology of the surface as they cancel out. Indeed, on a flat graphene sheet one can add two pentagons and two heptagons without changing the curvature of the molecule away from these deformations, as seen in Fig. 8(b). This is consistent with the effective gauge field description, where pentagons and heptagons have opposite flux contributions. On the other hand, non-trivial topologies necessarily introduce an imbalance between pentagons and heptagons. The genus zero configurations need an excess of pentagons, while high genus surface need an excess of heptagons. Genus one surfaces do not need any pentagons or heptagons at all as they are equivalent to a flat sheet.

As particular examples we see that Eqn. (13) reproduces the known case of a sphere with $g = 0$ that gives $\chi = 2$. This corresponds to the fullerenes that have $n_5 = 12$ and $n_7 = 0$. For the case of the torus we have $g = 1$ giving $\chi = 0$. Thus, no pentagons or heptagons are required. If one wants to consider the genus $g = 2$ surfaces then $\chi = -2$ for which $n_5 = 0$ and $n_7 = 12$. Fullerenes are compact surfaces, while the rest of the geometrical variants of graphene are usually defined on open surfaces. To apply our study to them we need to insert open boundary conditions to the Euler characteristic. This is simply achieved by considering the corresponding compact surface and introducing normal cuts to it. As an example, a torus with $g = 1$ can be cut along its small circle thus creating a cylinder with two open faces. The type of polygons between these two shapes is the same. So the generalization of the Euler theorem gives

$$n_5 - n_7 = 12(1 - g) - 6N, \tag{14}$$

where N is the number of open faces. The surgical procedure presented above, employed to produce open faces gives two open faces when the genus is reduced by one. In the case of nanotubes the surface has $g = 0$ and $N = 2$ that corresponds to $n_5 = n_7 = 0$. The case with $g = 0$ and $N = 4$ corresponds to two crossing nanotubes. In general, arbitrary configurations of genus g and of open faces N can be considered. Then the imbalance between the polygonal deformations is determined by relation (14). It remains to see how the total flux associated with the total number of pentagons and heptagons can determine the low energy spectrum of the molecule. In the next section we see how the index theorem can provide such an elegant relation.

5 The Atiyah-Singer index theorem

The index theorem gives an insight into the structure of the spectrum of certain operators, like the Dirac operator, without having to diagonalize them [8, 9, 10]. This information can be derived from general properties of the operators and the geometry of the space in which they are defined. In particular, the theorem is concerned with eigenstates that have zero eigenvalue, which in our case are the zero modes. Abstract as it might first sound it is not hard to follow a heuristic proof of the index theorem. Here we employ the approach based on the heat kernel expansion that provides the main elements, applicability and limitations of the theorem. The index theorem allows us to obtain a relation between the zero modes of the Dirac operator that corresponds to graphene and the total flux that goes through its surface. As the latter is related to the genus of the surface through the Euler characteristic we finally obtain, as promised, a relation between the zero modes and the topology of the surface.

Our starting point is a Dirac operator of the form

$$\not{D} = \begin{pmatrix} 0 & P^\dagger \\ P & 0 \end{pmatrix}, \tag{15}$$

where P is an operator that maps a space V_+ onto a space V_-, while $P^\dagger$ maps V_- onto V_+. If P is an $n \times m$ matrix, then $P^\dagger$ is a $m \times n$ matrix and V_+, V_- is the space of n, m dimensional vectors, respectively. For the Hamiltonian (8) obtained in the previous section, $\not{D}$ is one of the two sub-blocks of the diagonal differing by the sign in front of the gauge field, $\mathbf{A}$, P is a differential operator and $V_\pm$ is the space of complex functions.

As we are interested in the zero modes of $\not{D}$, i.e. the solutions of the equation $\not{D}\Psi = 0$, we can define the number of distinctive eigenstates of P with zero eigenvalue as ν_+ and the ones of $P^\dagger$ as ν_-. To facilitate the bookkeeping we introduce the chirality operator γ_5 as

$$\gamma_5 = \begin{pmatrix} 1 & 0 \\ 0 & -1 \end{pmatrix}. \tag{16}$$

Its eigenstates have eigenvalue ± 1 if they belong to $V_\pm$. To simplify our calculations we consider the operator $\not{D}^2$ that has the same number of zero eigenstates as $\not{D}$, but has the additional advantage of being diagonal

$$\not{D}^2 = \begin{pmatrix} P^\dagger P & 0 \\ 0 & PP^\dagger \end{pmatrix}. \tag{17}$$

It is possible to show that the operators $P^\dagger P$ and $PP^\dagger$ have the same non-zero eigenvalues. Indeed, if there is a state u such that $PP^\dagger u = \lambda u$, for eigenvalue $\lambda \neq 0$, then

$$PP^\dagger u = \lambda u \Rightarrow P^\dagger P(P^\dagger u) = \lambda(P^\dagger u), \tag{18}$$

which means that also the operator $P^\dagger P$ has the same eigenvalue, λ, corresponding to the eigenstate $P^\dagger u$. However, this is not necessarily the case for $\lambda = 0$ as $P^\dagger u$ could be zero by itself.

Let us now evaluate the following quantity

$$\mathrm{Tr}(\gamma_5 e^{-t\not{D}^2}) = \mathrm{Tr}(e^{-tP^\dagger P}) - \mathrm{Tr}(e^{-tPP^\dagger}) = \sum_{\lambda_+} e^{-t\lambda_+} - \sum_{\lambda_-} e^{-t\lambda_-}, \tag{19}$$

where λ_+ and λ_- are the eigenvalues of the operators $P^\dagger P$ and $PP^\dagger$, respectively, and t is just an arbitrary parameter. The first step in (19) is due to γ_5 acting on the exponential: it contributes a $+1$ to the eigenvectors of $P^\dagger P$, as they belong to V_+, and a -1 to the eigenvectors of $PP^\dagger$, as they belong to V_-. In the last step we evaluated the trace as a sum over all the eigenvalues of the corresponding operators. As we have shown, every non-zero eigenvalue of $P^\dagger P$ corresponds to an eigenvalue of $PP^\dagger$. Thus, all terms with non-zero eigenvalues cancel out in pairs and only the zero eigenvalues of each operator remain, finally giving

$$\mathrm{Tr}(\gamma_5 e^{-t\not{D}^2}) = \nu_+ - \nu_-. \tag{20}$$

The difference between the number of zero modes is in general undetermined. We call it the index of the $\not{D}$ operator, i.e. $\mathrm{index}(\not{D}) \equiv \nu_+ - \nu_-$. The above derivation provides us with an unexpected clue: due to the cancellation of the non-zero eigenvalue terms in (19) the expression $\mathrm{Tr}(\gamma_5 e^{-t\not{D}^2})$ is actually t independent!

What we just presented is merely a definition. Here, we are actually interested in finding out what is the value of $\mathrm{index}(\not{D})$. For that we shall employ an alternative way of calculating $\mathrm{Tr}(\gamma_5 e^{-t\not{D}^2})$ called the heat kernel expansion method [23]. It states that for a two dimensional compact surface and for general $\hat{f}$ and $\hat{D}$ operators one has the expansion

$$\mathrm{Tr}(\hat{f} e^{-t\hat{D}}) = \frac{1}{4\pi t} \sum_{k \geq 0} t^{k/2} a_k(\hat{f}, \hat{D}), \tag{21}$$

where Tr denotes the trace of matrices as well as the integration with respect to spacial coordinates and a_k are expansion coefficients. For $\hat{f} = \gamma_5$ and $\hat{D} = \not{D}^2$ we should obtain (20), that is an expression which is t independent. To achieve this, the coefficients a_k should be zero for all k except for $k = 2$ for which all the t contributions in (21) cancel out. The value of a_2 can be found from the first order term in the t expansion of the exponential. For this calculation we first evaluate that $\not{D}^2 = -g^{\mu\nu}\nabla_\mu \nabla_\nu + \frac{i}{4}[\gamma^\mu, \gamma^\nu] F_{\mu\nu} - \frac{1}{4}R$, where $F_{\mu\nu} = \partial_\mu A_\nu - \partial_\nu A_\mu$ is the field strength and ∇_μ is a covariant derivative with respect to gauge and reparametrization transformations. The magnetic field is given in terms of the field strength by $B_k = \frac{1}{2}\epsilon^{k\mu\nu} F_{\mu\nu}$. One can

now calculate that the non-zero expansion coefficient, a_2, is given by

$$a_2 = \mathrm{Tr}\Big\{\gamma_5\big(\frac{i}{4}[\gamma^\mu,\gamma^\nu]F_{\mu\nu} - \frac{1}{4}R\big)\Big\} = 2\iint \mathbf{B}\cdot d\mathbf{S}. \tag{22}$$

The integration in this equation runs over the whole surface. Combining the results from the two independent calculations of $\mathrm{Tr}(\gamma_5 e^{-t\not{D}^2})$ we have

$$\mathrm{index}(\not{D}) = \nu_+ - \nu_- = \frac{1}{2\pi}\iint \mathbf{B}\cdot d\mathbf{S}. \tag{23}$$

This is the final formula that demonstrates the index theorem. It relates the total flux that goes out of the surface to the number of zero modes of the $\not{D}$ operator. The curvature, R, does not appear in the index expression as γ_5 is a traceless operator. The absence of curvature is a characteristic of two dimensional surfaces. Finally, it is worth noting that Eqn. (23) makes sense only if the right hand side is an integer. This is indeed the case when we consider compact surfaces. Then $\iint \mathbf{B}\cdot d\mathbf{S}$ gives the total magnetic monopole charge inside the surface which takes discrete values due to Dirac's quantization condition of monopoles [24]. In the case of non-compact surfaces the theorem is applicable only when there is no flux going through the open faces.

6 Spectra of graphene molecules

In order to apply the index theorem to graphene and its geometrical variants we have to determine the contribution of the effective magnetic field to (23). As we have seen the effective magnetic field that appears in a certain graphene configuration, with minimally distorted lattices, is directly related to the genus of the graphene surface. In particular, we know that each pentagonal distortion in the honeycomb lattice gives rise to a specific circulation of the vector potential, namely $\oint_{C_p}\mathbf{A}\cdot d\mathbf{r} = \pi/2$, and similarly for heptagonal distortions. By employing Stokes's theorem we can relate the circulation of the gauge potential around a plaquette to the flux of the corresponding magnetic field. Indeed, we have

$$\oint_{C_p}\mathbf{A}\cdot d\mathbf{r} = \iint_{S_p}\mathbf{B}\cdot d\mathbf{S}, \tag{24}$$

where C_p is the looping trajectory for which the circulation of $\mathbf{A}$ is evaluated and S_p is the corresponding area. Thus, the total flux that goes trough the surface of the molecule can be evaluated if we know the total number of pentagons and heptagons. As heptagons contribute the opposite flux than pentagons we are only interested in the difference of their numbers. This is exactly determined by the genus of the surface through the Euler characteristic, i.e. $6\chi = n_5 - n_7 = 12(1-g) - 6N$. The total flux of the gauge field that goes through the surface of the molecule is, hence, given by

$$\frac{1}{2\pi}\iint_S \mathbf{B}\cdot d\mathbf{S} = \frac{1}{2\pi}\sum_{n_5-n_7}\oint_{C_p}\mathbf{A}\cdot d\mathbf{r} = \frac{1}{2\pi}\frac{\pi}{2}(n_5-n_7) = 3(1-g) - \frac{3}{2}N. \tag{25}$$

The total number of zero modes is the sum of the contributions from each sub-operator of H in (8). Consequently, we obtain the index of the Hamiltonian, H, that describes the molecule by adding these contributions. This finally gives

$$\mathrm{index}(H) = \nu_+ - \nu_- = 6(1-g) - 3N. \tag{26}$$

This is our final result that relates the number of zero modes present in a certain graphene molecule to the topological characteristics of its surface. Eqn. (26) gives us the minimum number of possible zero modes. The exact number is obtained from the index if either $\nu_+ = 0$ or $\nu_- = 0$. This actually holds for most of the cases when the index is non-zero.

We can now compare our results with the known cases of graphene molecules. For example, a fullerene has $g = 0$ and $N = 0$. Thus, it is expected to have six zero modes. This is indeed the case as the fullerenes have two triplet modes with energies very close to zero. For the case of a nanotube we have $g = 0$ and $N = 2$. This gives rise to index zero, which is in agreement with previous theoretical and experimental results [25, 26]. Nanotubes have either zero modes that satisfy $\nu_+ = \nu_-$ as happens for the armchair nanotubes (see Fig. 7(b)) or no zero modes at all, as it is the case for the zig-zag nanotubes (see Fig. 7(c)). The balance between the chiral zero modes is a consequence of the symmetry between the two directions along the nanotube that forces the two chiralities to be symmetric. Finally, the number of zero modes of more complicated molecules can be obtained from Eqn. (26).

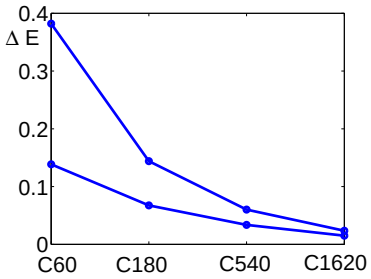

Figure 9. The low lying energy levels for the fullerenes C60, C180, C540 and C1620 obtained by direct diagonalization of their lattice Hamiltonians. Two triplets are obtained that correspond to the six zero energy modes in the continuum limit. As the size of the fullerene increases the energies of the low lying modes tend rapidly close to zero. The rest of the energy levels are separated with an energy gap of order one above and below the depicted energies. The energies are in units of the tunnelling coupling, J.

When comparing this to the spectra of real molecules one has to realize that small deviations are possible. Indeed, we have employed the continuous approximation in our derivation, while actual graphene molecules are defined on a lattice. Strictly speaking their lattice nature precludes them from having exact zero modes. Nevertheless, we expect to obtain low lying states that tend to zero modes when the molecule is taken to be larger and larger, thereby approximating the continuous limit better and better. This is clearly shown in Fig. 9, where the low lying spectra of the fullerenes C60, C180, C540 and C1620 are plotted. For each molecule two triplets are obtained corresponding to the six zero modes. This is as expected in the continuous limit with energies that approach rapidly zero as the size of fullerene increases. The rest of the spectrum is well separated from these low lying states.

This is a surprising relation between the topology and the spectrum of graphene molecules. In particular, it suggests that the zero modes need certain conditions in order to exist. An important ingredient is the presence of magnetic flux that is effectively inserted in graphene molecules by geometrical deformations. By inducing curvature with minimal distortions of the underlying lattice in the form of pentagons and heptagons we were able to relate the number of these deformations to the general topological characteristics of the lattice surface. This resulted in Eqn. (26) that relates the zero modes of a general graphene molecule with the genus and the number of open faces of its surface.

7 The next step: Vortices

The previously described topological effects are not the only ones that can be encountered in graphene. Recently, an inspiring relation between vortex-like topological defects and the number

of zero modes was demonstrated [27, 28, 29, 30, 31, 32]. This construction is not very different from the one we studied in the previous section. The crucial new element is the presence of a scalar field in the Dirac operator on which vortices can be encoded. This scalar field is generated in the effective picture by appropriate distortions of the tunnelling couplings of the graphene molecules. The main characteristic of the vortices is the presence of magnetic flux attached to them. The magnetic field associated with the vortices can be, in principle, introduced by external sources. Here we focus on the case where the field is generated by the geometrical deformations that we already introduced in the previous sections. This is a surprisingly simple mechanism compared to introducing external fields.

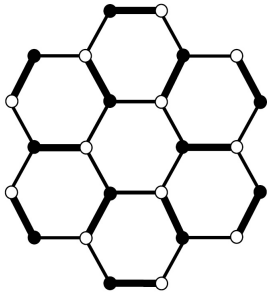

Figure 10. The Kekulé distortion introduced on the honeycomb lattice. A third of the hexagonal plaquettes has all the tunnelling couplings the same, while the rest two thirds of the hexagons have alternating strong and weak couplings.

Let us first see how the scalar field can appear in the effective low energy behavior of graphene. Consider a particular distortion of the tunnelling couplings of graphene, namely the Kekulé distortion, that is given by

$$\delta J_{\mathbf{r},k} = \frac{1}{3}\Phi(\mathbf{r})e^{i\mathbf{K}_+\cdot\mathbf{v}_k}e^{i(\mathbf{K}_+-\mathbf{K}_-)\cdot\mathbf{r}} + \text{c.c.}, \tag{27}$$

where Φ is a slowly varying function, $K_\pm$ are the Fermi points, $\mathbf{r}$ gives the position of the lattice sites and $\mathbf{v}_k$, for $k = 1, 2, 3$, indicate the positions of the three neighboring sites, as depicted in Fig. 4. It creates a pattern of weak, J, and strong, J', couplings as represented in Fig. 10. The effect of the distortion in the Dirac equation is to introduce a complex field, Φ, in the following way

$$H = \begin{pmatrix} -ie_k^\mu\sigma^k(\nabla_\mu - ieA_\mu) & \Phi \\ \Phi^* & ie_k^\mu\sigma^k(\nabla_\mu + ieA_\mu) \end{pmatrix}, \tag{28}$$

where $\Phi = |\Phi|e^{i2e\int \mathbf{A}\cdot d\mathbf{r}}$. As we see, the scalar field is directly coupled to the gauge field. The vorticity of the scalar field is defined as

$$\text{Vort}(\Phi) \equiv \frac{1}{2\pi}\oint_{\partial\Omega} d\mathbf{r}\cdot\boldsymbol{\partial}\text{Arg}\,\Phi = \frac{1}{4\pi i}\oint_{\partial\Omega} d\mathbf{r}\cdot\frac{\Phi^*\boldsymbol{\partial}\Phi - \Phi\boldsymbol{\partial}\Phi^*}{|\Phi|^2}. \tag{29}$$

It was argued by Jackiw and Rossi [33] and then proven by E. Weinberg [34, 35] that the index, which gives the zero modes of the Hamiltonian (28), is equal to the vorticity of the scalar field, i.e. $\text{index}(H) = \text{Vort}(\Phi)$. An extension of this theorem to compact surfaces was given in [30]. A direct calculation of the vorticity of the scalar field gives us

$$\text{index}(H) = \frac{1}{\pi}\iint_S \mathbf{B}\cdot d\mathbf{S}. \tag{30}$$

Note, that this index is with respect to four dimensional Hamiltonians in contrast to the pair of

two Dirac equations we encountered in the previous. The index is now twice the previous one reflecting the fact that the scalar field has twice the charge of the fermions, $2e$. The contour S is taken to enclose all vortices imprinted on the scalar field.

Chemists have long surmised that in fullerenes not all the nearest-neighbor hopping couplings are equal. In numerical calculations it is found that the molecules can lower their electronic energy by undergoing a Kekulé distortion. In particular, in the case of "leapfrog" fullerene molecules [36] C_{60+6k} with $k = 0, 1, ...$ it is possible to assign a Kekulé distortion in a consistent way. Thus, in addition to the gauge field that corresponds to the pentagons one obtains a scalar field from the possible coupling distortion.

From the previous study we know that the total effective magnetic flux of fullerenes is $3 \cdot 2\pi$. This property remains unchanged when a Kekulé distortion is introduced. The equality between vorticity (29) and the corresponding index (30) assign to the scalar field a total winding number of six. This is composed out of twelve half vortices attached to the twelve pentagons of the carbon lattice. The vorticity π of each vortex, instead of the flux $\pi/2$ of each pentagon, is due to the charge $2e$ that corresponds to the scalar field.

The index theorem applied to fullerenes with coupling distortion seems different than the one we employed for the undistorted molecules. However, both give the same total number of zero modes. This underlines the fact that introducing a scalar field in a Dirac operator does not change its total index. The only extra complication that arises is the angular discontinuity of the scalar field around the vortices due to their π vorticity. This forces us to introduce branch cuts, i.e. lines between pairs of vortices, where the scalar field takes zero value. Moreover, regularity of the vortices demands that the scalar field is smooth around the vortices.

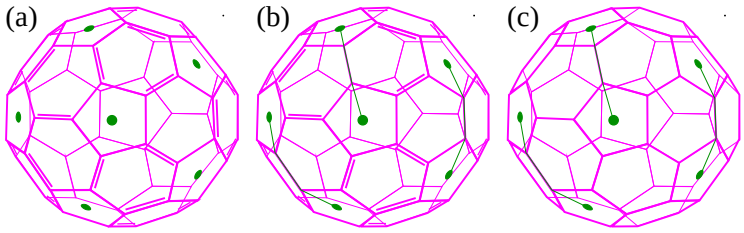

Figure 11. The coupling configuration of the C60 molecule, where vortices reside on the pentagons. (a) The Kekulé distortion. (b) Cuts between vortices are introduced by replacing a double bond with single ones. (c) An enlargement of the vortices is introduced by removing all double bonds connected to the pentagons. For C60 this removes all double bonds.

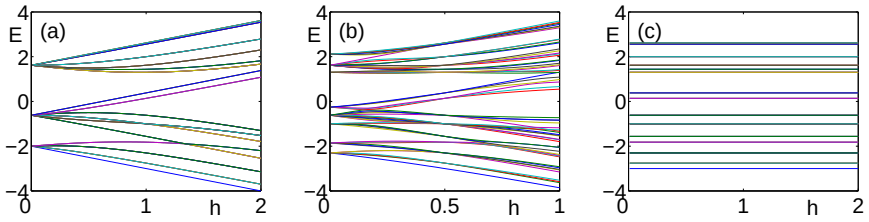

Figure 12. The spectrum of the C60 molecule as a function of the double bond coupling, h, with single bond coupling equal to 1. There are six modes (two triplets) that are near zero energy. (a) With Kekulé distortion. (b) With cuts between pairs of vortices. (c) With enlarged vortices, where all double bonds are removed.

In Fig. 11(a) we see the C60 fullerene with the Kekulé distortion depicted in terms of single and double bonds. The vortices are placed at the center of the pentagon plaquettes. In Fig. 11(b) branch cuts are introduced between connecting pairs of vortices. In Fig. 11(c) we increased the

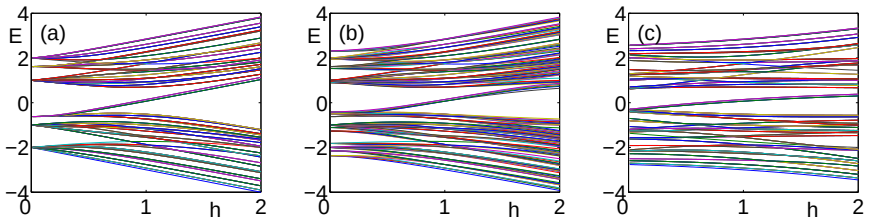

Figure 13. The spectrum of the C180 molecule. (a) With Kekulé distortion. (b) With cuts between pairs of vortices. (c) With enlarged vortices.

size of the vortices by removing the double bonds immediately connected to the pentagons. Fig. 12 shows the energy levels of the C60 fullerene as a function of the strength of the Kekulé distortion for the coupling configurations depicted in Fig. 11. In Fig. 13 the corresponding plots are presented for the C180 molecule. In both plots we see that two lines corresponding to two triplets have energies close to zero. These low lying states are interpreted as zero modes in the continuous limit. We clearly see that the insertion of branch cuts and the increasing of the size of the vortices makes the low lying energy states to be even closer to the zero energy. The difference of their energy from being exactly zero is due to the small size of the system. It is expected to converge to zero when larger molecules are employed [37].

To summarize, we showed that an effective scalar field is induced in the low energy description of graphene originating from a distortion in its tunnelling couplings. Importantly, the effective gauge field that originates from the insertion of pentagons and heptagons in the lattice couples directly to the scalar field imprinting vortices. As a result, the fullerene-type molecules have six half vortices. By employing the index theorem we demonstrated that there should be one zero mode for each pair of such vortices. While the effective gauge field is responsible for the presence of the zero modes the scalar field assures that the corresponding degenerate states are not locally distinguishable and remain localized around the vortex.

8 Charge fractionalization

The topological interplay between gauge and scalar fields in the relativistic description of graphene has, yet, another surprising consequence. It leads to the fractionalization of charge to the value $e/2$ for each 2π vortex. Thereby, it gives a natural setting, where topological effects, such as anyons, can emerge. The charge fractionalization is not an actual mechanical breaking of the electrons. It is rather a collective effect, appearing in the quantum state of the system, which conspires to assign half a charge to each vortex. In the case of finite systems fractionalized charges, $e/2$, should come in pairs as the total charge should always be an integer. This is the case as, for a compact system, 2π vortices came always in pairs. The fractionalization of charge is defined with respect to the difference between the electron density with and without the vortex. Nevertheless, it is not an uninteresting statistical effect that appears, e.g. due to averaging the wave functions that correspond to the presence and the absence of an electron. What actually happens is that the wave function of the system has fractional charge as an eigenvalue.

In this Section we present how the coupling between electrons and a vortex, as described in the previous section for graphene, gives rise to charge 1/2. For that we employ the quantum field theory description [38]. Consider the Dirac operator, $H(\Phi_{\rm v})$, with a scalar field that has a full vortex. The complete set of orthonormal eigenstates of the Hamiltonian is then given by $\Psi^{\rm v}_E$ parameterized by the energy eigenvalue E. The index theorem states that the presence of vortices gives rise to zero modes. We assume that our system with a *full* vortex has only a *single* zero mode, Ψ_0, related to it. We further assume that the eigenvalues E are symmetric around zero, i.e. the system possesses particle-hole symmetry. We also encountered this condition in Eqn. (18) of the index theorem.

In quantum field theory terms the state of the system is described by the quantum field

operator, $\hat{\Psi}$. For the case of a vortex this operator can be expanded in the eigenmodes of the corresponding Dirac operator, $\Psi^{\rm v}_E$, in the following way

$$\hat{\Psi}^{\rm v} = \sum_E (b_E \Psi^{\rm v}_E + d^\dagger_E \Psi^{\rm v}_{-E}) + a\Psi_0. \tag{31}$$

Due to the symmetry of the non-zero energy states, the modes $\Psi^{\rm v}_E$ and $\Psi^{\rm v}_{-E}$ can be paired. The first one appears with the particle annihilation operator, b_E, that acts on the conducting band and the second appears with the anti-particle creation operator, $d^\dagger_E$, that acts on the valence band. However, the zero mode does not have a partner. It is represented simply by the fermionic operator a. The zero mode, as all the fermionic modes, can be either occupied or empty. Since both states have zero energy, the zero mode has a double degeneracy. Denoting the empty zero mode state by $|-\rangle$ and the filled one by $|+\rangle$ we can represent the creation, $a^\dagger$, and annihilation, a, operators as

$$a|+\rangle = |-\rangle,\ a^\dagger|+\rangle = 0,\ a|-\rangle = 0,\ a^\dagger|-\rangle = |+\rangle. \tag{32}$$

In order to determine the total charge of the system we employ the charge operator, Q. This operator is given by

$$Q = \frac{1}{2}\int d^2x (\hat{\Psi}^\dagger\hat{\Psi} - \hat{\Psi}\hat{\Psi}^\dagger), \tag{33}$$

where the Schwinger's prescription is employed for its normalization. For the state (31) the charge operator becomes

$$Q^{\rm v} = \sum_E (b^\dagger_E b_E - d^\dagger_E d_E) + a^\dagger a - \frac{1}{2}. \tag{34}$$

Due to the balance between the energies in the conducting and valence bands, their contributions to the charge of half filled systems cancel out. Thus, the eigenvalues of the charge operator depend only on the state of the zero mode, giving

$$Q^{\rm v}|-\rangle = -\frac{1}{2}|-\rangle,\ Q^{\rm v}|+\rangle = \frac{1}{2}|+\rangle. \tag{35}$$

This demonstrates that the vortex charge is 1/2 in units of the electron charge! Note that in the absence of the zero mode the neutrality condition, $Q = 0$ would arise and no fractionalization would take place.

The above result demonstrates that the fractional value of the charge is indeed an eigenvalue of the charge operator. Our derivation was simply based on the spectral symmetry of the Dirac operator and the presence of the zero mode in the vortex sector, which is topological in its origin. Hence, the result is completely general regardless of the shape of the vortex or other details of the system. Fractional quanta of charge have been experimentally measured in the case of fractional quantum Hall effect [39, 40].

9 Anyonic statistics

The fractionalization of charge in two dimensions gives rise to another exotic effect. It makes it possible to realize anyons. The latter are quasiparticles, such as vortices, with fractional statistics that can range continuously from bosonic to fermionic. This is manifested by a non-trivial phase factor acquired by the state of two anyons when one is circulating the other, i.e. after two

successive exchanges, as seen in Fig. 14. In the case of bosons or fermions this phase factor would be 1 either arising from bosonic, $(+1)^2 = 1$, or from fermionic, $(-1)^2 = 1$, statistics. In the case of anyons, the phase resulting from two successive exchanges can actually take any

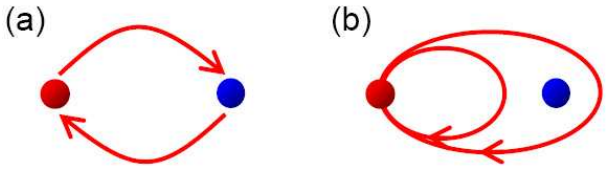

Figure 14. (a) Two quasiparticles are clockwise exchanged. The wave function of the quasiparticles is appropriately evolved according to their mutual statistics. (b) A succession of two exchanges gives rise to a single circulation of one particle around the other. In three spatial dimensions this circulation can be continuously transformed into a smaller loop and finally to a trivial one, where no circulation takes place. The latter evolution is equivalent to no transportation at all so the evolution operator should be the identity. Hence, the only possible exchange statistics is the bosonic, $(+1)^2 = 1$, or the fermionic, $(-1)^2 = 1$, as they are the only ones that give a trivial evolution after two exchanges.

complex value. This possibility arises in two dimensions. There, one can think of anyons as composite objects of a magnetic flux and an electric charge. Then the phase factor acquired by the circulation can be attributed simply to the Aharonov-Bohm effect. Indeed, the charge of one of the anyons circulates the flux of the other one, as seen in Fig. 15. The acquired phase factor depends only on the number of circulations and not on other characteristics of the path as expected from a statistical evolution.

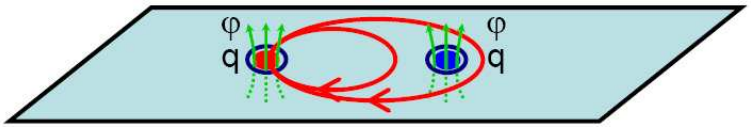

Figure 15. In two dimension two exchanges lead to a trajectory that cannot be continuously deformed to the identity one due to the presence of the circulated particle. Thus, an arbitrary phase factor, $e^{i\theta}$ could be assigned to this evolution giving rise to anyonic statistics. Intuitively, this can arise from attaching an effective integer flux, φ, to each anyon and an effective fractional charge q. Then the Aharonov-Bohm effect is responsible for the phase factor $e^{i\theta}$ acquired by the wave function.

Consider the case of graphene with Kekulé distortion in the tunnelling couplings. This gives rise to a scalar field that can support vortices. Suppose that vortices can appear with vorticity 2π. Then they will be accompanied by half a charge as we saw in the previous Section. Circulating such vortex around an identical one will give a phase factor π due to the Aharonov-Bohm effect,

$$q \iint_S \mathbf{B} \cdot d\mathbf{S} = \frac{1}{2} 2\pi = \pi.$$

This is a non-trivial phase that clearly demonstrates the anyonic nature of the vortices [41].

The generation and detection of anyons in graphene is an exciting subject of current research [27, 28, 29, 30, 31, 32]. If successful, it will give rise to a rich and versatile platform to perform experiments related to the fractional quantum Hall effect. Indeed, graphene offers several advantages, such as high electron mobility and resilience to temperature, that can prove valuable for probing these strongly correlated effects. Moreover, certain models with anyonic properties are of much interest in topological quantum computation. The latter promises to overcome the problem of environmental decoherence in the most efficient way.

10 Conclusions

In contrast to graphite, which is a rather soft substance, its constituent graphene layers have a robust lattice structure. This gives rise to graphene-based molecules that have a variety of

stable geometrical configurations, such as the fullerenes and the nanotubes. The predominant honeycomb lattice configuration of graphene is responsible for the effective relativistic behavior of its electrons. This behavior, combined with the long range quantum coherences present in graphene, allowed us to probe several exotic phenomena. Indeed, graphene and its geometrical variants provide an exciting laboratory for realizing numerous topological effects.

Initially, we saw how the low energy of graphene can be described by the relativistic Dirac operator. An effective magnetic field naturally appears whenever we introduce a geometrical deformation on the honeycomb lattice. This magnetic field is naturally coupled to the Dirac fermions allowing the emergence of phenomena already known from the quantum Hall effect. By considering the underlined lattice we were able to relate local geometrical characteristics of graphene to the general topology of the molecule by employing the Euler character. As a result, the celebrated index theorem provides insight into the spectrum of graphene molecules just by considering their topology. This theorem is able to predict, in a simple way, the number of zero modes that are present in the geometrical variants of graphene. We compared these results with the spectra of fullerenes and nanotubes and found remarkable agreement. The spectra of more complicated molecules can be also predicted with our formalism.

Subsequently, we considered the effect of tunnelling distortions on the relativistic properties of graphene. In particular, a scalar field emerges, on which vortices can be imprinted. An effective magnetic field due to distortions of the lattice geometry can create non-trivial vorticity on the scalar field. We analyzed this effect for the case of fullerenes, where tunnelling distortions are expected to appear due to the simultaneous presence of pentagonal and hexagonal plaquettes. An appropriately modified index theorem can be employed that correctly predicts the number of zero modes. The number of zero modes is unchanged when the tunnelling distortion is introduced. However, the wave functions of the zero modes are expected to become localized around vortices. This makes the exotic properties that accompany zero modes, such as the charge fractionalization, to become properties of the corresponding vortices.

The generation of vortices can also appear in flat graphene sheets. There vortices with 2π vorticity can be imprinted with the help of external magnetic fields. The resulting system behaves similarly to the fractional quantum Hall effect. The latter comprises of a continuum of two dimensional electrons at very low temperatures that are subject to a vertical magnetic field. There, vortices can support a variety of statistical behaviors. In the case of graphene we saw that the zero modes localized to vortices are responsible for the charge fractionalization as well as the emergent anyonic statistics of the vortices. It is an exciting perspective to realize such statistical phenomena with graphene. Its versatile behavior could prove valuable to technological applications of these many body effects.

Acknowledgements

This work was supported by the EU grants EMALI and SCALA, EPSRC and the Royal Society.

References

[1] A. K. Geim and K.S. Novoselov, Nature Materials **6**, 183 (2007).
[2] A. H. Castro Neto, F. Guinea, N. M. R. Peres, K. S. Novoselov and A. K. Geim, arXiv:0709.1163.
[3] P. R. Wallace, Phys. Rev. **71**, 622 (1947).
[4] K. S. Novoselov, A. K. Geim, S. V. Morozov,D. Jiang, Y. Zhang, S. V. Dubonos, I. V. Gregorieva and A. A. Forsov, Science, **306**, 666 (2004).
[5] M. I. Katsnelson, K. S. Novoselov, A. K. Geim, *Chiral tunnelling and the Klein paradox in graphene*, Nature Physics, **2** 620 (2006).
[6] K.S. Novoselov, A.K. Geim, S.V. Morozov, D. Jiang, M.I. Katsnelson, I.V. Grigorieva, S.V. Dubonos, and A.A. Firsov, Nature 438, 197 (2005); K.S. Novoselov, E. McCann, S.V. Morozov, V.I. Falko, M.I. Katsnelson, U. Zeitler, D. Jiang, F. Schedin, and A.K. Geim, Nature Physics, 2, 177 (2006).
[7] K. S. Novoselov, Z. Jiang, Y. Zhang, S. V. Morozov, H. L. Stormer, U. Zeitler, J. C. Maan, G. S. Boebinger, P. Kim, and A. K. Geim, Science **315**, 1379 (2007).

[8] M. F. Atiyah and I. M. Singer, Ann. of Math. **87**, 485 (1968); Ann. of Math. **87**, 546 (1968); Ann. of Math. **93**, 119 (1971); Ann. of Math. **98**, 139 (1971); M. F. Atiyah and G. B. Sigal, Ann. of Math. **87**, 531 (1968).
[9] T. Eguchi, P. B. Gilkey, and A. J. Hanson, Phys. Rep. **66**, 215 (1980).
[10] M. Stone, Ann. Phys. **155**, 56 (1984).
[11] J. K. Pachos and M. Stone, Int. J. Mod. Phys. B, 21, 5399 (2007).
[12] J. K. Pachos, A. Hatzinikitas and M. Stone, Eur. Phys. J. Special Topics **148**, 127 (2007).
[13] G. K. Brennen and J. K. Pachos, Proc. R. Soc. A 10.1098/rspa.2007.0026 (2007).
[14] Y. Aharonov and D. Bohm, Phys. Rev. **115** 485 (1959).
[15] D. P. DiVincenzo and E. J. Mele, Phys. Rev. B **29**, 1685 (1984).
[16] J. Gonzalez, F. Guinea, M. A. H. Vozmediano, Nucl. Phys. B **406**, 771 (1993).
[17] V.A. Osipov, E.A. Kochetov, JETP Letters **73**, 631 (2001).
[18] D. V. Kolesnikov and V. A. Osipov, Eur. Phys. J. B **49**, 465 (2006).
[19] P. E. Lammert, and V. H. Crespi, Phys. Rev. Lett. **85**, 5190 (2000); Phys. Rev. B **69**, 035406 (2004).
[20] H. W. Kroto, J. R. Heath, S. C. O'Brien, R. F. Curl and R. E. Smalley, Nature **318**, 162 (1985).
[21] L. V. Radushkevich and V. M. Lukyanovich, J. Phys. Chem. **26**, 88 (1952).
[22] See for example, Imre Lakatos, Proofs and Refutations, Cambridge Technology Press (1976).
[23] D. V. Vassilevich, Phys. Rept. **388**, 279 (2003).
[24] S. Coleman, The Magnetic Monopole Fifty Years Later, in The Unity of the Fundamental Interactions (Plenum Press, New York, 1983).
[25] S. Reich, C. Thomsen, and P. Ordejon, Phys. Rev. B **65**, 155411 (2002).
[26] R. Saito, M. Fujita, G. Dresselhaus, and M. S. Dresselhaus, Phys. Rev. B **46**, 1804 (1992).
[27] C.-Y. Hou, C. Chamon, and C. Mudry, Phys. Rev. Lett. **98**, 186809 (2007).
[28] R. Jackiw and S.-Y. Pi, Phys. Rev. Lett. **98**, 266402 (2007).
[29] C. Chamon, C.-Y. Hou, R. Jackiw, C. Mudry, S.-Y. Pi, and A. P. Schnyder, Phys. Rev. Lett, **100**, 110405 (2008).
[30] J. K. Pachos, M. Stone, and K. Temme, Phys. Rev. Lett. **100**, 156806 (2008).
[31] P. Ghaemi and F. Wilczek, arXiv:0709.2626 (2007).
[32] B. Seradjeh, H. Weber, and M. Franz, arXiv:0806.0849.
[33] R. Jackiw and P. Rossi, Nucl. Phys. B **190**, 681 (1981).
[34] E. J. Weinberg, Phys. Rev. D **24**, 2669 (1981).
[35] C. Callias, Commun. Math. Phys. **62**, 213 (1978).
[36] P. W. Fowler, M. Fujita, M. Yoshida, J. Chem. Soc. Faraday Trans. **92** 3763 (1996).
[37] J. Gonzalez, F. Guinea, M. A. H.Vozmediano, Phys. Rev. Lett. **69**, 172 (1992).
[38] R. Jackiw, math-ph/0503039.
[39] D. C. Tsui, H. L. Stormer, and A. C. Gossard, Phys. Rev. Lett. **48**, 1559 (1982).
[40] V. J. Goldman, and B. Su, Science **267**, 1010 (1995).
[41] B. Seradjeh and M. Franz, arXiv:0709.4258 (2007).